Title
Study of Anti-Tarnishing Mechanism in Ag-In Binary System by Using Semi-Quantum-Mechanical Approach

Journal
Journal of The Electrochemical Society, 164(7)

ISSN
0013-4651

Authors
Huo, Yongjun
Wu, Jiaqi
Lee, Chin C

Publication Date
2017

DOI
10.1149/2.1471707jes

Journal of The Electrochemical Society, **164** (7) C418-C427 (2017)
0013-4651/2017/164(7)/C418/10/$37.00 © The Electrochemical Society

Study of Anti-Tarnishing Mechanism in Ag-In Binary System by Using Semi-Quantum-Mechanical Approach

Yongjun Huo,[a,b,z] Jiaqi Wu,[a,b] and Chin C. Lee[a,b]

[a]*Department of Electrical Engineering and Computer Science, University of California, Irvine, California 92697, USA*
[b]*Materials and Manufacturing Technology, University of California, Irvine, California 92697, USA*

Tarnishing of silver objects have been real issues throughout millennia of human civilization history due to the fact that silver is very susceptible to sulfur element and can easily get tarnished by sulfur-containing gases. Over the past several decades, researchers have been studying mechanisms of tarnishing phenomena and tried to formulate and develop anti-tarnishing engineering solutions for various fields of applications, including jewelry, catalysts, electronics and optics. Recently, our research group demonstrated that silver-indium solid solutions possessed excellent anti-tarnishing property by quantitative experimental studies. However, the anti-tarnishing mechanism in silver-indium binary system is still unknown. In this paper, anti-tarnishing mechanism in silver-indium binary system is studied by a semi-quantum-mechanical approach. Silver-indium thin film were systematically examined by several experimental approaches in order to study their crystallography and surface properties thermodynamically. An original semi-quantum-mechanical approach was introduced for calculating the Hard and Soft Acids and Bases quantifiable parameters based on conceptual DFT formalization and incorporated with the Hammer-Nørskov d-band model, namely, absolute electronegativity and chemical hardness. Finally, the discovery of increasing absolute electronegativity and chemical hardness can be used to theoretically interpret the most fundamental mechanism behind the mystery of anti-tarnishing phenomenon in the silver-indium binary system.

Manuscript submitted March 22, 2017; revised manuscript received May 25, 2017. Published June 3, 2017.

Silver was used for coins in ancient Lydia around 700 BC,[1] but still finds new special niches of technological applications, such as silver thin films,[2–4] silver nano-particles,[5–9] and silver nano-sintering.[10,11] It possesses superior material properties, such as the highest electrical conductivity of any element, the highest thermal conductivity and reflectivity among metals, reasonable price and truly remarkable aesthetic value.

However, silver is very sensitive to the presence of sulfur-containing corrosive gases such as sulfur vapor,[12] hydrogen sulfide,[13] sulfur dioxide,[14] and organic sulfur vapors,[15] etc., even for very low concentrations ranging from less than 1 parts per billion (ppb) in normal atmosphere to hundreds of ppb in heavy industrial environments. Therefore, pure silver can easily get tarnished and form silver sulfide after a period of time, resulting in degradation of original electrical[16] or optical performance[17] or rendering long-term reliability[18] of its products at stake.

In order to understand the nature of silver sulfurization, a considerable number of research has been conducted over the decades. For example, several environmental parameters, such as temperature, relative humidity,[19] illumination,[14] and surface states,[20] have been studied to explore the silver tarnishing mechanism based on electrochemical models. In order to search possible scientific and engineering anti-tarnishing solutions, some surface treatment techniques for silver have been proposed, using different coating methods or coating materials, such as metallic coating by electroplating,[21] sputter-applied coatings,[22] oxide coating,[23] organic coating,[24] chromate conversion coating.[25] However, such thin layers of coating material can be worn out very easily after a period of time. Another approach to address tarnishing issues for silver is by alloying. It has been reported that adding other elements such as palladium,[26] silicon,[27] tin,[28] germanium,[29] and zinc,[30] can be effective, more or less, for anti-tarnishing purposes.

Recently, the authors studied the tarnishing reactions of pure silver and silver-indium solid solutions with sulfur vapor (S_8).[31] The experimental results showed that silver-indium solid solutions exhibited a superior anti-tarnishing property, which could be meaningful to various fields of silver applications, such as jewelry, catalyst, welding, electronics, and optics. However, the anti-tarnishing nature of silver-indium solid solutions and the underlying mechanism were not discussed in that paper.

In the present work, the anti-tarnishing mechanism in silver-indium binary system is addressed in a theoretical and systematical manner. Essentially, silver tarnishing is a corrosion phenomenon which is largely related to solid-gas interfacial reactions. Therefore, anti-tarnishing should be one of the intrinsic properties of silver-indium solid solutions surface. Accordingly, it is appropriate to study its fundamental physical-chemistry with surface sensitive techniques. X-ray photoelectron spectroscopy (XPS) and ultraviolet photoelectron spectroscopy (UPS) are experimental techniques whose capabilities can fulfill the tasks for probing the physical-chemical properties determined by core-level electrons and valence band electronic structures.

The preparation and characterization of Ag-In thin film samples is presented followed by the nature of metallic surfaces of silver-indium alloy as indicated by the XPS and UPS experimental results. A systematic review of the Hard and Soft Acids and Bases (HSAB) principle is presented along with its conceptual Density Functional Theory (DFT) formalization, and Molecular Orbital Theory (MOT). The experimental results are discussed within the framework of the HSAB principle. An alternative methodology, which is incorporated with the Hammer-Nørskov d-band model, is proposed to calculate HSAB parameters for bulk metals. Finally, a physical-chemical model is proposed to explain the anti-tarnishing mechanism in the silver-indium binary system, based on experimental evidence and self-contained theoretical analysis.

Material Preparation and Characterization

E-beam evaporation process.—The methods to grow ingots of silver-indium solid solution phase bulk material for characterizing its mechanical properties were shown previously.[32] Polishing can damage and contaminate samples surface, and alter the original material surface properties. However, XPS and UPS are highly surface sensitive experimental techniques. Therefore, bulk material samples might not be suitable to the current study. Instead, high quality thin film samples of silver-indium solid solution phase (α phase) with same compositions of our previous study are used.

E-beam evaporation was chosen for the preparation of thin film samples of pure silver, silver-indium solid solution phase, Ag_9In_4 intermetallic compound (IMC) in Ag-In binary system. The raw materials of pure silver and indium shots with 99.99 wt% purity were weighed, uniformly mixed and loaded in a graphite crucible for the following E-beam evaporation. In this study, the compositions of starting raw materials were carefully adjusted in order to obtain the desired composition of Ag-In alloys thin film samples. 1 inch × 1 inch squares of fused quartz with 1 mm thickness were mounted on the substrate stage of the evaporator as the deposition substrates of the thin film samples. The evaporation chamber was pumped down to 2×10^{-8} torr before turning-on the E-beam source, and then the materials in

[z]E-mail: yongjunh@uci.edu

crucible were pre-soaked for 5 mins with swirling pattern of E-beam in order to completely melt the target materials. During the E-beam evaporation process, the deposition rate was monitored by a quartz crystal microbalance (QCM), and was controlled at 1 Å/s ± 5%, using a proportional–integral–derivative (PID) controller. The substrate stage was in-plane rotating constantly at 60°/s during the deposition to ensure the uniformity of the resulting thin film samples. The resulting thickness of silver-indium thin film samples was 100 nm ± 5%.

Grazing incidence X-ray diffraction characterization.—The fabricated thin film samples were further examined with a Rigaku SmartLab X-ray diffractometer, using parallel beam (PB) mode to perform grazing incidence X-ray diffraction (GIXRD). The grazing angle of incidence (Ω) is optimized at 0.65° in order to achieve optimal intensity of GIXRD signal. The GIXRD is performed from 20° to 90° at scanning speed of 1°/min, using collimated Cu K_α line excitation X-ray source. After GIXRD measurement, the collected data were analyzed by PDXL, an integrated powder X-ray analysis software package, and compared with The International Centre for Diffraction Data (ICDD) standard card.

X-ray photoelectron spectroscopy.—The AXIS Supra by Kratos Analytical at the UC Irvine Materials Research Institute (IMRI) was used to perform the experimental XPS/UPS characterization for the resulting thin film samples. X-ray photoelectron spectra (XPS) were recorded with a monochromatized Al Kα radiation source ($\hbar\omega$ = 1486.6 eV) under ultra-high vacuum (UHV) operated below 1×10^{-8} torr. The analyzed spot size was 300 μm × 700 μm, with an analyzer pass energy of 20 eV. All of the XPS survey spectra were obtained by scanning of the analyzer using step of 1 eV with a dwell time of 300 ms, and the recorded survey spectra can be used for quantification analysis. The XPS regions spectra were obtained by using scanning step of 0.05 eV with dwell time of 300 ms, and a sufficiently large number of sweeps for each region was recorded to achieve reasonable signal-to-noise ratio. The gas cluster ion source (GCIS) system inside the AXIS Supra was used to clean the sample surface with Ar+ ions in order to remove any form of surface contamination and native oxide while maintaining at UHV, thereby preventing the surface from any further contamination or oxidation after the surface cleaning.

Ultraviolet photoelectron spectroscopy.—The silver-indium alloys valence band electronic structure is needed to understand the mechanism behind the dramatic lowering of the chemical reactivity with sulfur gas molecule (S_8) found previously.[31] Ultraviolet photoelectron spectroscopy (UPS) investigates the electronic structures of valance bands, and it provides higher photoionization cross sections and fourfold higher energy resolution compared to XPS.[33] Although UPS spectral shapes are often incident photon energy dependent, the spectra generally converge to the same one and start to resemble the occupied density of states (DOS), i.e., electronic density distribution, of the measured valance bands for photon energy $\hbar\omega > 40$ eV. Accordingly, the monochromatized resonance radiation source from He II ($\hbar\omega$ = 40.8 eV) of the AXIS Supra was chosen to conduct the UPS experimental measurement on the silver-indium alloy valance bands structure. The analyzer energy resolution was set as high as 0.01 eV, and a sufficiently large number of sweeps for each spectrum was recorded to achieve good signal-to-noise ratio for the measurement data. The inherent energy resolution of the UPS measurement was 0.095 eV, which was determined from the width of the Fermi edge of pure Ag thin film sample. The raw data of the measurement were smoothed by 10 adjacent point averaging algorithm, thereby not significant lowering the UPS inherent energy resolution.

Experimental

Grazing incidence X-ray diffraction results.—The GIXRD pattern of pure silver, silver-indium solid solutions with different compositions, and Ag_9In_4 IMC thin film samples have been plotted in Fig. 1. The intended values of indium concentration of the silver-indium

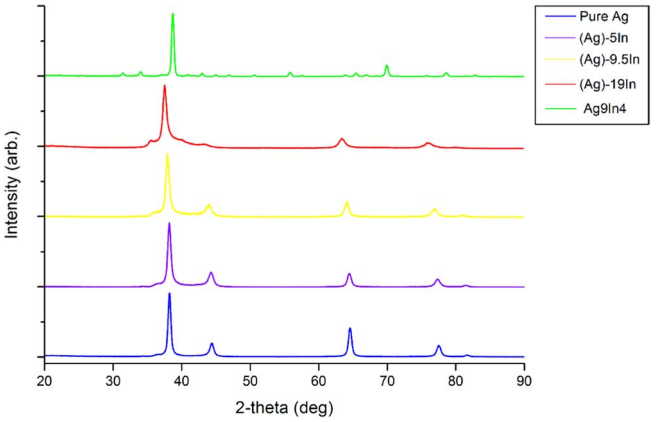

Figure 1. GIXRD patterns of the Ag-In thin film samples.

solutions thin film samples were 5 at. %, 9.5 at. % and 19 at. %, which were nominally designated as (Ag)-5In, (Ag)-9.5In and (Ag)-19In, in order to correlate with the tarnishing experimental reaction rates measured in our previous study.[30] The weighted average values for lattice constants are 4.082 Å, 4.094 Å, 4.109 Å and 4.145 Å for pure silver and each silver-indium solid solutions thin film sample. In addition, the silver-indium binary system should obey Vegard's Law, i.e., the lattice constant changes linearly as the solute concentration increases within its solid solution range.[34] As shown in Fig. 2, the calculated average lattice constants of bulk samples in previous study and of thin film samples in this study are plotted together with ICDD standard powder samples of silver and silver-indium solid solutions. The lattice constants of silver-indium solid solutions of bulk material samples data were measured in our previous study,[32] and they increase linearly with the increase of indium concentration.

As shown in Fig. 2, the linear fitting curve of bulk material lattice constants is nearly parallel and above the linear curve determined by ICDD data points. Next, we used the nominal indium concentration values of silver-indium solid solutions thin samples to plot another curve in Fig. 2. As a result, resulting lattice constants data points of thin samples fitted well with the increasing linear relationship, and their linear fitting curve is also nearly parallel but under the linear curve of ICDD powder samples. Thus, we can safely confirm that nominal indium concentrations were near true values of silver-indium solid solutions thin film samples. Additionally, if ICDD powder

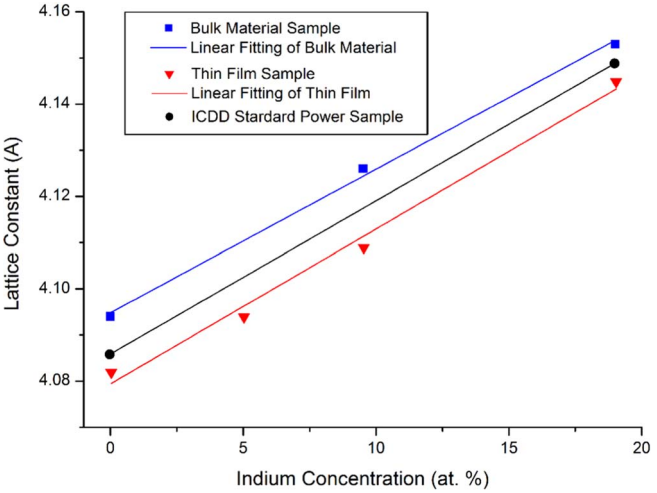

Figure 2. The plot of calculated average lattice constants of Ag-In bulk samples, thin film samples and ICDD standard powder samples with linear fitting curves.

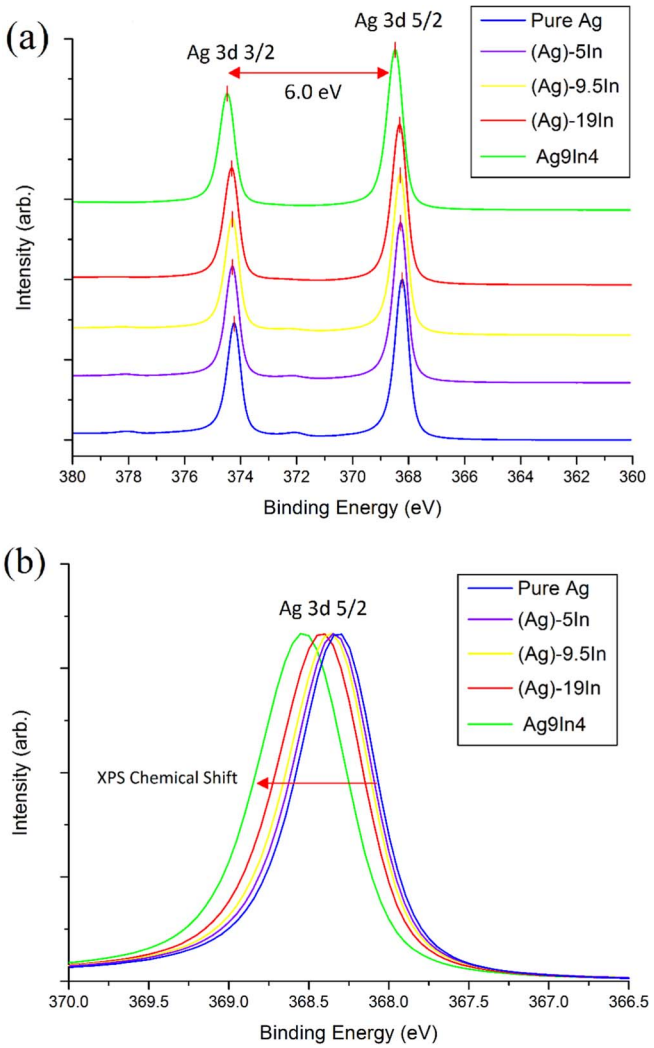

Figure 3. (a) X-ray photoelectron spectra of Ag 3d region, (b) chemical shift of Ag 3d 5/2 peaks of Ag-In thin film samples.

samples were considered stress-free samples, the bulk materials grown in house should exhibit macroscopic residual tensile stress, and the thin film samples should exhibit macroscopic residual compressive stress to explain the reason why their linear curves shifted upwards and downwards, respectively, in Fig. 2.

For Ag_9In_4 IMC sample, 24 peaks in GIXRD pattern were recognized by PDXL, 23 peaks among them were identified with Ag_9In_4 phase except for the one minor peak. Ag_9In_4 IMC exhibits a complex crystal structure in the cubic system with P-43m space group symmetry. The most intensive peak is centered at 38.69°, which corresponds to the (3 3 0) crystal plane, according to ICDD standard card No. 01-071-0128. Therefore, it can be safely confirmed that the resulting Ag_9In_4 IMC thin film is single phase material, without any other phases in the silver-indium binary system. In the supplementary material, GIXRD patterns with more details and crystallographic information were provided.

In summary, pure silver, silver-indium solid solutions and Ag_9In_4 IMC thin film samples have been successfully fabricated for further XPS/UPS study, with the confirmation of GIXRD phase identification. It is worthwhile noticing that several minor peaks in GIXRD patterns of native metallic oxides have been also identified, and it will be discussed in the following section.

X-ray photoelectron survey spectra results.—In the supplementary material, the XPS survey spectra of all thin film samples were provided. After quantification analysis of CasaXps, the cleaned surface composition of the samples can be precisely determined with sensitivity as high as 0.01 at. %, using intensity and areas of survey spectral peaks in Ag 3d and In 3d regions. The results showed that the indium concentration were 5.32 at. %, 9.86 at. %, 19.70 at. % and 32.43 at. % for each Ag-In solid solutions and Ag_9In_4 IMC respectively. Therefore, it is conclusive to confirm that the thin film samples compositions were well-controlled within 1 at. % error of tolerance, verifying that nominal notations for the thin film samples were indeed valid.

Table I. A summary of Ag 3d regions spectral peaks position, FWHM and chemical shift of Ag-In thin film samples.

	Ag 3d 3/2 (eV)		Ag 3d 5/2 (eV)		
Compositions	BE	FWHM	BE	FWHM	Chemical Shift (eV)
Pure Ag	374.30	0.60	368.30	0.58	-
(Ag)-5In	374.35	0.62	368.35	0.60	0.05
(Ag)-9.5In	374.35	0.63	368.35	0.62	0.05
(Ag)-19In	374.40	0.67	368.40	0.64	0.10
Ag_9In_4	374.55	0.69	368.55	0.67	0.25

X-ray photoelectron Ag 3d regions spectra results.—Fig. 3 shows the Ag 3d region spectra for all of the cleaned thin film samples. All of measured spectral peaks positions were calibrated against the pure Ag 3d 5/2 peak at E_b = 368.30 eV, which is the reference level from the instrument manufacturer for monochromatic Al K_α X-ray source excitation, and the spectral intensities were normalized with the highest peak in each spectra. The Ag 3d region peaks were labeled in each spectrum, and the peak positions are summarized in Table I. As shown in Fig. 3a, the Ag 3d 3/2 and 5/2 peaks exhibits typical Doniach-Sunjic asymmetric lineshape[35] with unchanged spin-orbit splitting energy of 6.0 eV for all thin film samples, which is in agreement with the high energy resolution results of pure Ag 3d regions spectra in the literature.[36]

As shown in Table I, the peaks position of Ag 3d 3/2 and 5/2 have both shifted to higher binding energy, and the full width at half maximums of both peaks have increased with the increase of indium concentration of the thin film samples. Fig. 3b shows a continuous trend of peak shifting in Ag 3d 5/2 peaks regions of silver-indium solid solutions and Ag_9In_4 IMC, where (Ag)-5In, (Ag)-9.5In and (Ag)-19In exhibit small chemical shifts of 0.05 eV and 0.10 eV, respectively, with respect to pure Ag. The measured chemical shift of Ag_9In_4 IMC is 0.25 eV, which is relatively large compared to that of silver-indium solid solutions. This is understandable since its crystallography has changed from FCC to complex cubic superlattice crystal structure, so that the chemical environment of Ag atoms in the IMC would be altered drastically.

In the literature,[37] the chemical shift measured by XPS was also referring as core-level shift (CLS), which is different from the shift of the core-electron eigenstates (initial state CLS) by the amount of the core hole relaxation energy (ΔE_R). The core hole relaxation process will contribute to the shift from the remaining electrons as they were screened by the charge imbalance caused by the core hole, and it is often known as final state effects. However, in many cases, the final state effects are often assumed to be independent of the chemical environment, and therefore do not contribute to the core-level chemical shift. A more detailed approach in analyzing core-level chemical shift can be rationalized by using the calculation scheme through the Born-Haber cycle.[38] Several important physical and thermodynamic properties of alloys, such as cohesive energy,[39] heat of mixing,[40] segregation energy,[41] etc. can be estimated from the core-level chemical shift analysis by this approach. It can be concluded that the Ag 3d core-level electrons of silver-indium alloy exhibited typical core-level electrons character, and were well-screened from the outside environment.

Table II. A summary of O 1s regions spectral peaks position of Ag-In thin film samples.

Binding Energy (BE)	Ag-O (eV)	Relative Intensity (%)	In-O (eV)	Relative Intensity (%)	Doublet Splitting (eV)
Pure Ag	530.4	100%	-	-	-
(Ag)-5In	530.9	100%	529.1	26%	1.8
(Ag)-9.5In	531.2	100%	529.3	43%	1.9
(Ag)-19In	531.2	100%	529.5	60%	1.7
Ag_9In_4	532.3	100%	530.3	88%	2.0

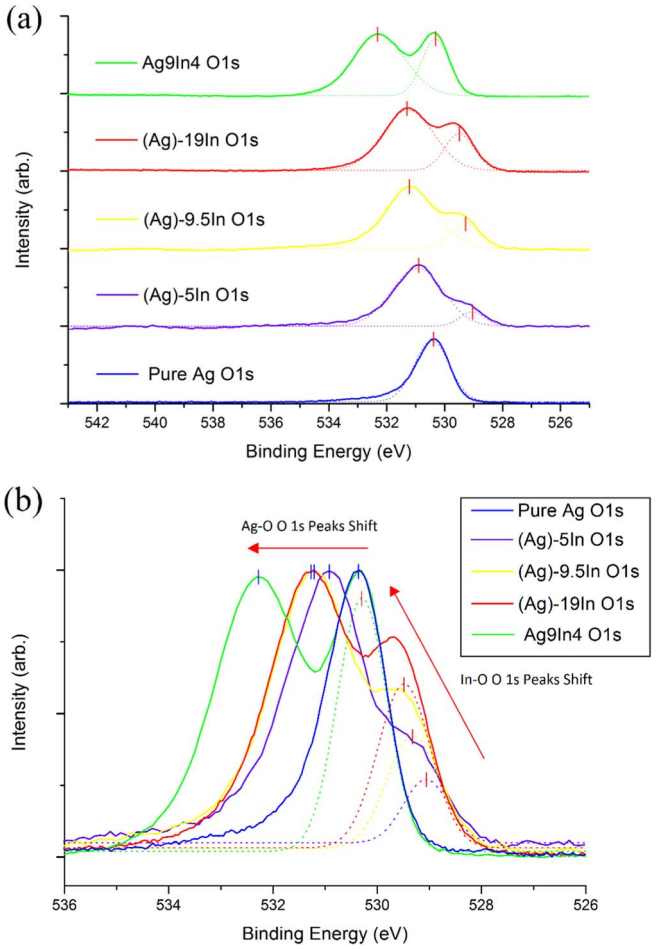

Figure 4. (a) X-ray photoelectron spectra of O 1s region, (b) the trend of O 1s region major peaks shift of Ag-In thin film samples.

X-ray photoelectron O 1s region spectra results.—The natural oxidation state of the original silver-indium alloy surface is largely correlated with the various interfacial chemical reactions. Therefore, XPS O 1s region spectra were measured for the as-deposited thin film samples without Ar+ ion cleaning. The resulting XPS O 1s region spectra were plotted with solid lines, and fitted with Gaussian lineshape using dot-lines for each major peaks for all thin film samples in Fig. 4, with intensity normalized against the highest peak in each spectrum. As shown in Fig. 4a, the O 1s region spectra for as-deposited pure silver thin film sample has one major peak at E_b = 530.4 eV, which corresponds to atomic oxygen with Ag-O bonding character.[42] A hump appears at the lower binding energy side of the original major peak in the O 1s region spectrum of the (Ag)-5In thin film sample, and the original major peak of O 1s shifts toward the higher binding energy side to E_b = 530.9 eV. After deconvolution and fitting with a Gaussian lineshape, the peak position and relative intensity of the emerging peak can be determined, which is at E_b = 529.1 eV and of 26% intensity of original major peak. The major characteristic O 1s peak of pure In_2O_3 is known to be at E_b = 529.5 eV, and the peak position would shift if other doping elements were involved.[43] Therefore, this emerging O 1s might correspond to In-O bonding character with Ag element involved in its local chemical environment. Accordingly, as shown in Fig. 4b, the trend continues as the indium concentration of the thin film samples increases: the relative intensity of In-O bonding character O 1s peak increases; both Ag-O and In-O bonding character peak positions shift toward higher bonding energy. It is worthwhile noticing that the shift of Ag-O bonding character from (Ag)-9.5In to (Ag)-19In is negligible, meaning the chemical environment of atomic oxygen with Ag-O bonding character remains almost the same for silver-indium solid solutions with high indium concentration. In addition, the amount of peak shift from solid solutions to IMC is relatively large so that the chemical environment of atomic oxygen is quite different from solid solutions to IMC surfaces. In Table II, the peak position, relative intensity, and energy splitting of the two major peaks were summarized. Based on the experimental results above, it is clear that atomic oxygen experiences two different chemical environment, namely, Ag-rich and In-rich, in the naturally formed oxide layers of silver-indium solid solutions and IMC, and the percentage of In-rich oxide increases with the indium concentration of the alloy increases, reaching about the same level of Ag-rich oxide for Ag_9In_4 IMC thin film sample.

Ultraviolet photoelectron spectra results of valence bands.—In the literature,[44] indium had an s2p1 outer valence shell electronic configuration, and it was reported that In 4d spectral peaks (E_b = 16 – 18 eV) exhibited core-level electron character. The charge transfer between In 4d energy level and Ag 4d-band is negligibly small, so that the In 4d energy level is well-separated from the Ag valence bands. Therefore, the energy was scanned from E_b = 15.8 eV to Fermi energy level for the UPS valence bands measurement. Fig. 5a shows the smoothed UPS spectra of thin film samples. Their binding energy started from 11 eV, beyond which no features showed up other than inelastic scattering background. Each Ag valence 4d-band UPS spectrum of Ag-In thin film samples could be divided into two parts, which were designated as primary 4d-bands and secondary 4d-bands. Several features are evident from the UPS smoothed spectra. First of all, the Ag overall 4d-bands moved to higher binding energy, which agreed with the general trend in Ag-In binary system UPS spectra described in the literature.[45] Secondly, the indium 5s valence level signal showed up at higher binding energy end of spectra and they were well-separated from Ag 4d-bands. The Fermi energy edges and Ag 5s-bands were clearly observed and labelled in the UPS spectra.

It is essential to remove the background signal of inelastic scattering and obtain normalized UPS spectra for further quantitative study. In bulk Ag, Ag 5s electrons mixed with 4d electrons to a large extent in the valence band, which began at E_b = 7.5 eV and extended all the way to the edge of Fermi energy. In the literature,[46] the distribution of Ag 5s electrons exhibited a shallow terrace form, and their contributions to valence band were negligibly small. In addition, it is also hard to distinguish 5s valence electrons apart from inelastic electrons. Therefore, the Ag 5s-bands were removed together with the inelastic background, thereby investigating Ag 4d-bands exclusively for each spectrum. Discarding the s-band and considering only the d-band electrons, it is in accordance with the valence band data treatment method in the Hammer-Nørskov (HN) d-band model.[47,48] In the HN d-band model, for the transition metals (TMs) the s-band is half-full,

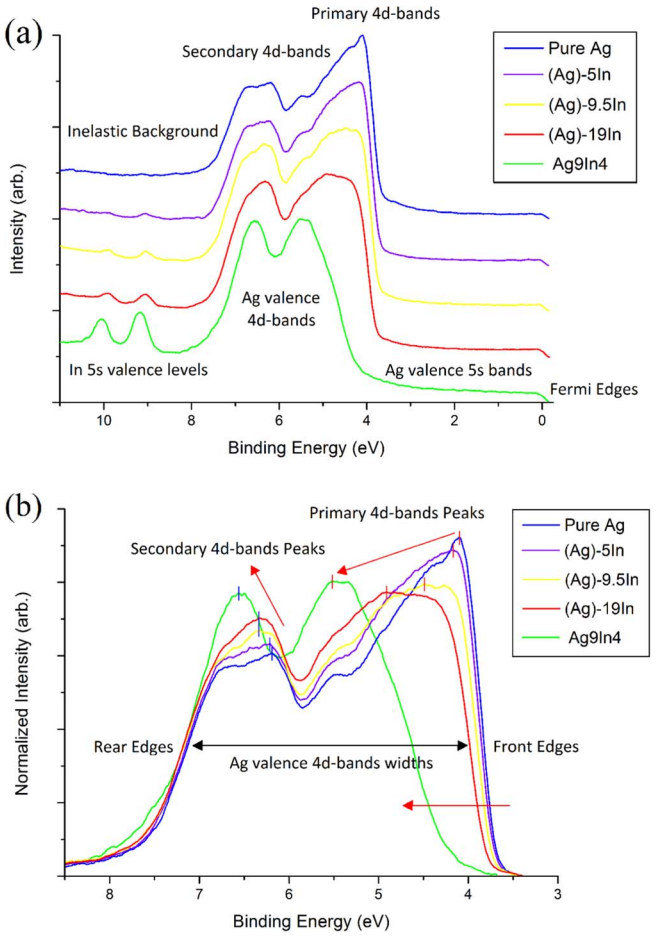

Figure 5. (a) Ultraviolet photoelectron spectra of valence bands, (b) normalized spectra of Ag valence 4d-bands of Ag-In thin film samples.

and correspondingly the reactivity of TMs is given by the position of the d-band. It has been proved that Hammer-Nørskov d-band model is very useful and effective theoretical quantum-mechanical modelling method in predicting noble and late transition metallic catalyst behavior.

Furthermore, each spectrum was normalized against the total number of electrons in the valence bands. Fig. 5b shows the normalized Ag valence 4d-bands with primary and secondary 4d-bands peaks and band-widths labelled. The features of the normalized UPS spectra, namely, primary and secondary 4d-band peak positions, front edges and rear edges of Ag valence 4d-bands and band-widths, were listed in Table III. The front edges of Ag valence 4d-bands shifted away from Fermi energy level with the increase of indium concentration. Moreover, primary 4d-bands peaks exhibited an even larger amount of shifting. In contrast, not only the amount of secondary 4d-bands peaks shift was relatively small, but also the rear edges of the Ag valence 4d-bands were almost pinned, therefore largely narrowing the band-widths. In addition, in terms of normalized intensity, its d states were localized at the top of the valence band for pure Ag,[36] which is directly confirmed in Fig. 5b. However, the normalized intensities of primary 4d-bands decreased for Ag-In solid solutions spectra as the indium concentration increased, whereas secondary 4d-bands intensity increased with the addition of indium solutes. Therefore, the occupied valence states become less localized at the top of valence band, and a prominent charge transfer phenomenon, from primary bands to secondary bands, occurred. In conclusion, the electronic distribution of Ag 4d-bands were largely affected by adding indium solute into the original silver crystal lattice, and would further lead to a great impact on chemical behavior. In the following section, the correlation between the Ag-In valance bands electronic structures to their chemical behaviors is discussed within the framework of the HSAB principle.

HSAB Principle and Discussion

HSAB principle and its conceptual density functional theory formalization.—In early days, R.G. Pearson had categorized Lewis acids and bases as either hard or soft, and established hard and soft acids and bases (HSAB) principle based on experimental facts: *hard acids react preferentially with hard bases, and soft acids react preferentially with soft bases*.[49] This statement refers to the generalized acid-base reaction shown in Eq. 1, where A is the Lewis acid, electron acceptor or electrophile, B is the Lewis base, electron donor or nucleophiles, and A:B is an acid–base complex, an adduct, or a coordination compound. It is worthwhile noticing that one reactant could act as Lewis acid in one chemical reaction and act as Lewis base in another chemical reaction, depending on whether it would accommodate electrons or donate electrons in that particular chemical reaction.

$$A+ : B \rightarrow A : B \qquad [1]$$

The HSAB principle has been proved to be useful in inorganic[50] and organic chemistry.[51] One of the great successes of the HSAB principle is to rationalize the experimental fact that silver (soft base) is relatively chemical inert to oxygen (hard acid) in the atmosphere, but can be easily tarnished by sulfur element containing gases (soft acids), whereas classic reduction–oxidation (redox) theories failed to interpret those phenomena appropriately. In essence, the HSAB principle is phenomenological in its nature, which means that there should be underlying theoretical reasons to explain the chemical facts which this principle summarizes. Intuitively, the ionic–covalent theory would be able to give qualitative explanations for the HSAB principle: hard acids and hard bases tend to form ionic character (coulomb attraction) molecular bonding, whereas soft acids and soft bases tend to form covalent character (orbitals hybridization) molecular bonding in their resulting acid–base complex. Those hard–hard or soft–soft chemical interactions are generally more favored energetically, so that their acid–base complex is also chemically and thermally stable. Particularly, some transition metals with loosely held outer d-orbital electrons, especially Ag, are willing to share their valence electrons with empty outer orbitals available on other basic atoms, such as sulfur and iodine, to form covalent bonding and lower their orbital energy by d-p hybridization of their molecular orbitals.[52] This is supported by the π-bonding theory of Chatt[53] and the d-p orbital hybridization mechanism proposed by Mulliken.[54] On the other hand, for example, silver oxide (Ag_2O) has much lower melting temperature (300°C)

Table III. A summary of normalized UPS spectra characteristic information of Ag-In thin film samples.

Binding Energy (eV)	Primary 4d-band Peak	Secondary 4d-band Peak	Front Edge	Rear Edge	Band Width	Primary 4d-band Peak Shift	Front Edge Shift
Pure Ag	4.10	6.19	3.84	7.06	3.22	-	-
(Ag)-5In	4.17	6.21	3.87	7.07	3.20	0.07	0.03
(Ag)-9.5In	4.49	6.33	3.92	7.09	3.17	0.39	0.08
(Ag)-19In	4.91	6.33	4.01	7.10	3.09	0.81	0.17
Ag_9In_4	5.52	6.56	4.68	7.10	2.42	1.42	0.84

compared to most metal oxides and it would even decompose at 200°C. Thus it is clearly not thermally nor chemically stable. Because silver oxide is essentially a hard acid–soft base complex, its molecular bonding is at a transition state between ionic character and covalent character, which results in an energetically non-favorable electronic configuration.

However, the HSAB principle was criticized earlier because of the lack of a strict mathematical deduction or parameters to quantify this kind of material property.[55] Fortunately, Parr has introduced quantifiable parameters into the HSAB principle scheme, namely, chemical hardness and softness.[56] In addition, Kohn and Sham (K-S) have developed the density functional theory (DFT)[57] as a computational quantum-mechanical modelling method, thereby allowing people to describe and explain the HSAB phenomena in a more mathematically rigorous and systematical manner. Within the K-S framework of DFT, one would be able to compute with a set of self-consistent equations, and acquire calculated results of electron density distribution, n(r), total number of electron, N[n(r)], and total ground state electronic energy, E[n(r)], for a chemical system of finite atomic number (100–200). Generally, the resulting E vs. N plots are usually convex upward curves, and their slopes and curvatures represent two parameters of substantial importance, electronic chemical potential (μ) and chemical hardness (η), as shown in Eq. 2 and Eq. 3:

$$\mu = (\partial E/\partial N)_v = -\chi_M \quad [2]$$

$$\eta = \left(\partial^2 E/\partial N^2\right)_v = (\partial \mu/\partial N)_v \quad [3]$$

$$\sigma = (\partial N/\partial \mu)_v = 1/\eta, \quad [4]$$

where v is the potential due to the nuclei, uniquely determined by n(r). The definition of chemical softness, σ, is given by Eq. 4, which is the reciprocal of chemical hardness.

The electronic chemical potential characterizes the escaping tendency of electrons from the equilibrium system,[58] and it is exactly the negative value of the absolute electronegativity in the Mulliken scale (χ_M). In the Lewis acid–base reaction (Eq. 1), the total energy (E) and chemical potentials (μ) of the acid (A) and base (B) reactants can be expanded into Taylor series. The resulting equations, Eq. 5 and 6, can be derived by setting the chemical potentials of A and B, i.e., $\mu_A = \mu_B$, equal to each other.

$$\Delta N = \frac{(\mu_{B^0} - \mu_{A^0})}{(\eta_A + \eta_B)} = \frac{(\chi_{A^0} - \chi_{B^0})}{(\eta_A + \eta_B)} \quad [5]$$

$$\Delta E = -\frac{1}{2}(\mu_{B^0} - \mu_{A^0})\,\Delta N = -\frac{1}{2}\frac{(\mu_{B^0} - \mu_{A^0})^2}{(\eta_A + \eta_B)} = -\frac{1}{2}\frac{(\chi_{A^0} - \chi_{B^0})^2}{(\eta_A + \eta_B)} \quad [6]$$

Where the superscript zero refers to the original reactants states and the total number of charge transfer is $\Delta N = N_A - N_{A^0} = N_{B^0} - N_B$ and total energy change due to charge transfer $\Delta E = (E_A - E_{A^0}) + (E_B - E_{B^0})$. When the chemical potentials of A and B are equal to each other, the thermo-equilibrium state can be reached and the net charge transfer process between two reactants will stop. Parr[56] presented this conceptual DFT formalization for the HSAB principle.

Obviously, the acid must be more electronegative than the base to drive the electron transfer process, and the total energy of the system will be lower as a result of electron charge transfer. Physically, the chemical hardness can be regarded as the resistance to the electron charge transfer process. If both the acid and base are soft, then the denominator, $\eta_A + \eta_B$, would be a small number. If they have also a reasonable difference in electronegativity, e.g. sulfur and silver, the resulting ΔN and ΔE in Eq. 5 and Eq. 6 would be substantial, which mathematically demonstrates that soft acid–soft base interactions facilitate the electron charge transfer to form covalent bonding and substantially lowering total energy of the system. For a hard acid–hard base combination, the electron charge transfer should be small, but it can stabilize system by energy-favorable electrostatic interactions, namely, ionic bonding.

However, the derivatives of Eq. 2 and 3 were historically ill-defined[59] due to the "integer discontinuities".[60] Thus, the electronic chemical potential and chemical hardness are usually calculated for practical applications by the finite-difference approximation, shown in Eq. 7 and Eq. 8, where I is ionization potential and A is the electron affinity.

$$\mu = -\frac{I + A}{2} < 0 \quad [7]$$

$$\eta = I - A \geq 0 \quad [8]$$

It is also important to correlate the HSAB principle with molecular orbital theory (MOT) since it is one of the well-established theories and has been accepted and widely used by chemists. One can establish the bridge by Eq. 9, according to Koopmans' theorem:

$$-\varepsilon_{HOMO} = I, \qquad -\varepsilon_{LUMO} = A \quad [9]$$

Where ε_{HOMO} is the frontier orbital energy of highest occupied molecular orbital (HOMO) and ε_{LUMO} is the frontier orbital energy of lowest unoccupied molecular orbital (LUMO). Combining Eqs. 7–9, it is easy to see that electronic chemical potential is the midpoint of energy HOMO and LUMO frontier orbitals, and chemical hardness is the energy gap between HOMO and LUMO. Note that Koopmans' theorem is only valid within the Hartee-Fock theory so that DFT calculated ε_{HOMO} and ε_{LUMO} are rather poor approximations for -I and –A.[61] In summary, the HSAB principle has been proven to be self-contained and can be quantatively and theoretically formalized using conceptual DFT. Therefore, the HSAB principle and its DFT conceptual formalization should be valid and useful in explaining or predicting molecular or aqueous based chemical reactions.

HSAB parameters calculation for bulk metals.—Bulk metals seemed to have the same chemical hardness, $\eta = 0$, since their ionization potential equals to electron affinity (I = A). Historically, this I = A, which leads to $\eta = 0$, was well-known and had been often acknowledged in the literature.[56] In solid state physics, the corresponding term of HOMO–LUMO gap is the bandgap between valence band and conduction band. For bulk metals, the valence band overlaps with conduction band, so the bandgap would be zero, which is equal to the chemical hardness of bulk metals. However, experiments show that there is a large difference exists in terms of chemical reactivity in reactions with soft acids (e.g. sulfur element containing gases) for different bulk metals, even for those with similar electronegativity (e.g. silver vs. copper[62]). Therefore, it would be questionable whether the finite-difference approximation is still suitable for chemical hardness calculation of bulk metals within the HSAB and its conceptual DFT framework. In the literature, Yang and Parr[63] showed that when the temperature is at absolute zero (T = 0 K), the chemical hardness of bulk metals was actually related to the inverse of their density of states at Fermi energy, which was an extremely small number. More recently, some attempts had been made to establish HSAB models for bulk metals and surfaces, incorporating work functions and Fermi energy for parameterization.[64,65] The established HSAB model[65] is valid in predicting the charge transfer and reaction between bulk metal and reactive atomic adsorbates (strong Lewis acids), namely, N, O, and Cl. However, S element and sulfur molecules were not mentioned in that model. Therefore, the original definitions of electronic chemical potential and chemical hardness, given by Eq. 2 and Eq. 3, were used to establish a theoretical model based on HSAB and conceptual DFT by different approach, namely, incorporating with Hammer-Nørskov d-band model.

As an alternative method to the DFT quantum-mechanical computation, the electronic distribution for valence bands can be obtained from high-precision measurements. The XPS regions spectra show that the core-level electrons are well-screened and separated from the outside environment, so their influence on chemical reactions

in terms of charge transferring would be negligible small. Therefore, only the valence band electrons were considered for HSAB parameters calculation.

With normalized UPS measurement data of Ag valence 4d-bands, i.e., the DOS of the 4d-bands, $n_d(\varepsilon)$, total ground state electronic energy in 4d-bands, $E_d[\varepsilon]$, and total number of electrons in 4d-bands, $N_d[\varepsilon]$, can be readily calculated through the approach of numerical integration of the experimental data by using Eq. 10 and Eq. 11:

$$N_d(\varepsilon) = \int_{-\infty}^{\varepsilon} n_d(\varepsilon')\, d\varepsilon' \approx \sum_i n_d(\varepsilon_i)\, w \qquad [10]$$

$$E_d(\varepsilon) = \int_{-\infty}^{\varepsilon} \varepsilon' n_d(\varepsilon')\, d\varepsilon' \approx \sum_i \varepsilon_i n_d(\varepsilon_i)\, w \qquad [11]$$

Where w is the step width of the numerical integration, and ε_i is the local electronic energy, which is equal to negative value of the binding energy of valence band electrons. The Eq. 10 is known as the integrated-density-of-states, and the Eq. 11 is known as the moment of the d-band.[48] These two equations together have been used to calculate the center of the d-band by integrating over the whole d-band within the scheme of the Hammer-Nørskov d-band model.[47,48] This calculation approach is in agreement with the local density approximation (LDA) in the DFT framework.

By using this approach, it can be assumed that the UPS spectra approximately resemble the nature of electronic distribution in their corresponding valence bands. This methodology should be more accurate than a finite-difference approximation in calculating the electronic chemical potential and chemical hardness for bulk transition metals. In spite of the UPS spectra being measured from thin film samples, thermodynamically, those thin film samples should still be considered as bulk metals, as compared with molecules or nanoclusters. In addition, care must be taken when computing E vs. N curves for HSAB consideration, since not all of the electrons in the Ag valence 4d-bands would contribute to the hybridization process in forming covalent bonding with soft acids molecular orbitals. As a result, the primary Ag valence 4d-bands were used to construct the E vs. N curves due to fact that those electrons are at higher energy states (lower binding energy) and most likely to participate in the acid–base reactions, i.e., hybridizing with LUMOs of molecules of sulfur element containing gases to form covalent bonds.

Fig. 6 shows the normalized total electronic energy vs. the normalized total number of electrons in 4d-bands, E vs. N, curves of thin film samples, using the methodology described above, and the calculated HSAB quantifiable parameters, i.e., absolute electronegativity, chemical hardness, and chemical softness, were listed in Table IV. In Fig. 6, the energies are all negative with zero energy high up on top. The numerical integration values for the total number of electrons are the same for all curves, and the values of the total number of electrons are normalized to a constant. Since the numerical integration values of total number of electrons and total electronic energy are correlated, the averaged slopes and curvatures of curves are invariants to the normalization constant, which guarantees that the resulting HSAB quantifiable parameters are exact as defined in Eq. 2 and Eq. 3. First of all, as listed in Table IV, all of the resulting chemical harnesses have small but non-zero positive values, which demonstrates that the results are consistent with earlier non-zero estimation of chemical hardness for bulk metals.[63] The chemical hardness values are larger than previous results due to the fact that the authors discarded s-band electrons and considered d-band electrons only in UPS data post-possessing. Secondly, as depicted in Fig. 6, the change of E vs. N curves from pure Ag to (Ag)-5In is negligible small, so the difference in terms of electro-negativity is only 0.02 and calculated chemical hardness and softness of (Ag)-5In remain as the same values of pure Ag. This indicates that dilute concentration of indium element solutes would not significantly alter the original valence band electronic structure of silver, nor the thermodynamic properties. In contrast, the trend of increasing electronegativity and chemical hardness with the increase of indium concentration is prominent for heavily doped silver-indium solid solutions, (Ag)-9.5In and (Ag)-19In. Significantly, there is a large increase of absolute electronegativity and chemical hardness for Ag_9In_4 IMC, so that one would expect a fundamental change of its thermodynamic and chemical properties. In the following section, the correlation between the HSAB parameters and anti-tarnishing property in silver-indium binary system is demonstrated.

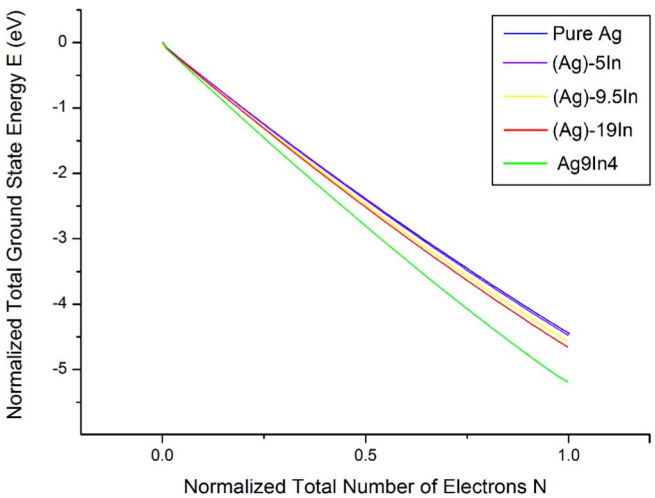

Figure 6. The plot of the normalized total ground state energy vs. the normalized total number of electrons in 4d-bands curves of Ag-In thin film samples.

Table IV. A summary of absolute electronegativity, chemical hardness, and chemical softness of Ag-In thin film samples and molecular gases.

	χ_M (eV)	η (eV)	σ (eV^{-1})
Pure Ag	5.03	0.24	4.1
(Ag)-5In	5.05	0.24	4.1
(Ag)-9.5In	5.21	0.26	3.8
(Ag)-19In	5.33	0.27	3.6
Ag_9In_4	6.00	0.32	3.1
S_2	5.51	3.85	0.26
H_2S	4.20	6.20	0.16
O_2	6.30	5.90	0.17

Anti-Tarnishing Mechanism

In the literature,[50] absolute electronegativity and chemical hardness of S_2, H_2S, and O_2 molecular gases were calculated by using finite-difference approximation, and these values are listed in Table IV. Several qualitative theoretical predictions can be made through comparisons with the calculated values of absolute electronegativity. First of all, the oxygen molecule can oxidize all thin film samples since its absolute electronegativity is higher, and this has been experimentally proved by the previous GIXRD and XPS experimental results. Secondly, the absolute electronegativity of hydrogen sulfide molecule is lower than that of pure Ag, so it predicts that H_2S molecular gases cannot spontaneously react with pure Ag or Ag-In alloy alone. This is also an experimental fact which has been demonstrated in early days by several chemists,[66] showing that H_2S gases will not tarnish Ag without the help of moisture and oxidizing agents. The value of absolute electronegativity of S_2 molecules sits between that of (Ag)-19In and Ag_9In_4 IMC, so it predicts that sulfur gases can still slightly tarnish Ag-In solid solutions, but will not tarnish Ag_9In_4 IMC at all. By inserting values in Table IV into Eq. 5, the calculated result of ΔN for Ag_9In_4 should be larger in magnitude than that of (Ag)-19In, but it has a negative value. The negative value of ΔN implies that

Table V. A summary of calculated total charge transfer and energy lowering of reactions with S_2 molecule and experimental reactions rates with S_8 molecule.

	ΔN (%)	ΔE (%)	R (%)
Pure Ag	100	100	100
(Ag)-5In	95.8	91.8	-
(Ag)-9.5In	62.2	38.8	28.6
(Ag)-19In	37.2	3.4	4.4
Ag_9In_4	0	0	0

the charge transfer would flow reversely, namely, from HOMOs of sulfur molecules to Ag 4d-band of Ag_9In_4. However, the Ag 4d-band has been already completely filled, therefore, the electrons in sulfur element or molecules cannot flow into 4d-band in order to form stable covalent bonds. This implies that the roles of Lewis acid and Lewis base in the reaction between S molecules and Ag-In alloy cannot interchange in order to form a stable acid–base complex. Therefore, the reaction rate between Ag_9In_4 IMC and S molecules can be considered to be zero. Note that above arguments should be only valid for noble metals with full-filled d-bands. To check on the validity of this theoretical prediction, a separated tarnishing experiment was performed, using an Ag_9In_4 thin film sample and exactly the same experimental setup and parameters with 60 mins duration as described previously.[31] Under such serve tarnishing environment, pure Ag would definitely grow a thick black layer of Ag_2S and Ag-In solid solutions would be blacken slightly on the surface. The prediction is accurate, i.e., the Ag_9In_4 thin film sample is completely anti-tarnishing, showing exactly the same shining silvery mirror surface as before the tarnishing experiment. This confirms that the methodology used in calculating absolute electronegativity and chemical hardness for bulk metals is accurate and consistent with the scale of previous calculated HSAB parameters.

The tarnishing rates of (Ag)-9.5In and (Ag)-19In were found previously to be 3.5 times and 22.8 times, respectively, slower than that of pure Ag in the reaction experiment with sulfur vapor (S_8) within a closed system.[31] With those values of electronegativity and chemical hardness at hands, it is easy to calculate nominal total number of charge transfer, ΔN, and total energy lowering, ΔE, of chemical reactions between sulfur vapor and Ag, Ag-In solid solutions and Ag_9In_4 IMC by using Eq. 5 and Eq. 6. Note χ_M- χ_{S2} was set to zero if $\chi_M > \chi_{S2}$ so that ΔN and ΔE would be both equal to zero. The reason to justify this treatment was given above previously. As a result, the calculated values of ΔN and ΔE in reactions with S_2 molecule were listed, together with experimental reactions rates with S_8 molecule, in Table V, normalized with data value of pure silver. Those calculated values exhibited highly non-linear characters from which logistic functions can be extrapolated, and they were plotted as logistic fitting curves in Fig. 7. As shown in Fig. 7a, tarnishing reactions rates, total number of charge transfer and total amount of energy decrease with the increase of indium concentration. The trend of decrease for tarnishing reaction rates and energy lowering is highly correlated, therefore the drop of energy lowering in the process of charge transfer could be the underlying reason for the anti-tarnishing property in Ag-In binary system. The calculation results are largely in agreement with the theoretical predictions given by the Hammer-Nørskov d-band model, which states that the lower is the center of the d-band (ε_d), the less reactive is the surface,[48] which is evident from Fig. 5b. The data points of energy lowering can be fitted into the following logistic function, shown in Eq. 12:

$$\Delta E\,(x) = \frac{100}{1 + (x/t)^k} + 0.11 \qquad [12]$$

Where x is the indium concentration (at. %) of Ag-In thin film samples and t and k are both fitting constants which have the numerical values of 8.57 and 4.42 respectively.

As depicted in schematic diagrams, shown in Fig. 7, the tarnishing and anti-tarnishing mechanism in the Ag-In binary system can be described as following:

As shown in Fig. 7b, when silver crystal is exposed to an environment containing sulfur vapor (S_8), the sulfur molecules (adsorbates) can be brought into intimate contact with the surface of silver (adsorbent) through the process of chemical adsorption, during which original sulfur molecules might dissociate into smaller ones (S_2-S_7) or even elemental form (S). Upon the moment of the contact, a strong tendency of electron charge transfer would occur from the top of valence band of Ag solid to empty outer orbitals of sulfur element, i.e., LUMOs, which results in forming Ag-S covalent bonds by the orbital hybridization process and in substantially lowering the overall energy of the system. When $\Delta E > 0$, the forward reaction is thermodynamically favorable. The amount of energy released by the orbital hybridization process can be contributed to overcoming the energy barrier of the growth of Ag_2S, thereby facilitating breaking of the original chemical bonds, nucleation, atomic migration and rearrangement. Therefore, the silver can be easily tarnished by sulfur vapor and the sulfurization reaction is both energetically and kinetically favorable.

On the contrary, as shown in Fig. 7c, when silver formed a solid solution with indium solute, the valence electrons become less localized at the top of the valence band. The electronic valence band structures keep on changing and contracting inwards with the increase of indium solute concentration, which results in increasing its absolute electronegativity and chemical hardness. During the sulfurization reaction, the tendency of electron charge transfer from the valence band to LUMOs is largely reduced and the total amount of energy lowering become much smaller. The change of ΔE will affect the chemical process in terms of overcoming the energy barrier of the chemical reaction, thereby affecting the reactivity and kinetics of the sulfurization reaction. Therefore, even though the sulfurization reaction is still thermodynamic favorable, the tarnishing rates of Ag-In solid solutions are substantially suppressed due to the fact that much less energy releases from the electron charge transfer process. In other words, the tarnishing reaction becomes less kinetically favorable, which leads to much less tarnishing rates of Ag-In solid solutions. The prediction of the reactivity of Ag-In metal surface is essentially in agreement with the Hammer-Nørskov d-band model.

Furthermore, as shown in Fig. 7d, when silver-indium has formed intermetallic as the indium concentration increases, it has fundamentally changed the crystallography and thermodynamic properties. The valence electrons of IMC are much less localized at the top of valence band and the band structure is further contracted inwards, which results in its absolute electronegativity value becoming even higher than that of the sulfur vapor molecules. Even though the majority of atoms in Ag_9In_4 lattices are still silver, there is a very limited tendency of electron charge transfer between the LUMOs of sulfur molecules and the Ag 4d-band of Ag_9In_4, due to the resulting modified Ag valence band structure. When the $\Delta E \leq 0$, the change in terms of Gibbs free energy of the forward reaction should be greater than zero, so that the reaction cannot proceed spontaneously. Therefore, the tarnishing reaction has become thermodynamically unfavorable, so that Ag_9In_4 IMC is completely anti-tarnishing to sulfur vapor.

It must be considered that a very thin atomic layer metallic oxide exists on the surfaces of bulk metal. As seen in the XPS results, the fact of O 1s core-level shifting toward higher binding energy indicates that metallic oxide on the surface becomes more chemically stable and the percentage of In-rich metallic oxide is also increasing with indium concentration in the bulk metal. Since indium oxide will not react with sulfur vapor, the thin metallic oxide layers should also contribute to the anti-tarnishing property. However, the silver sulfide layers grown on both pure Ag and Ag-In solid solutions exhibit linear growth,[31] which implies that those sulfurization processes are kinetically limited only by the reaction rate at the growth sites, so it is reaction-controlled rather than diffusion-controlled. Therefore, no continuous metallic oxide layer forms to act as passivation layer or diffusion barrier to shield the silver from tarnishing gases and correlate metallic oxide

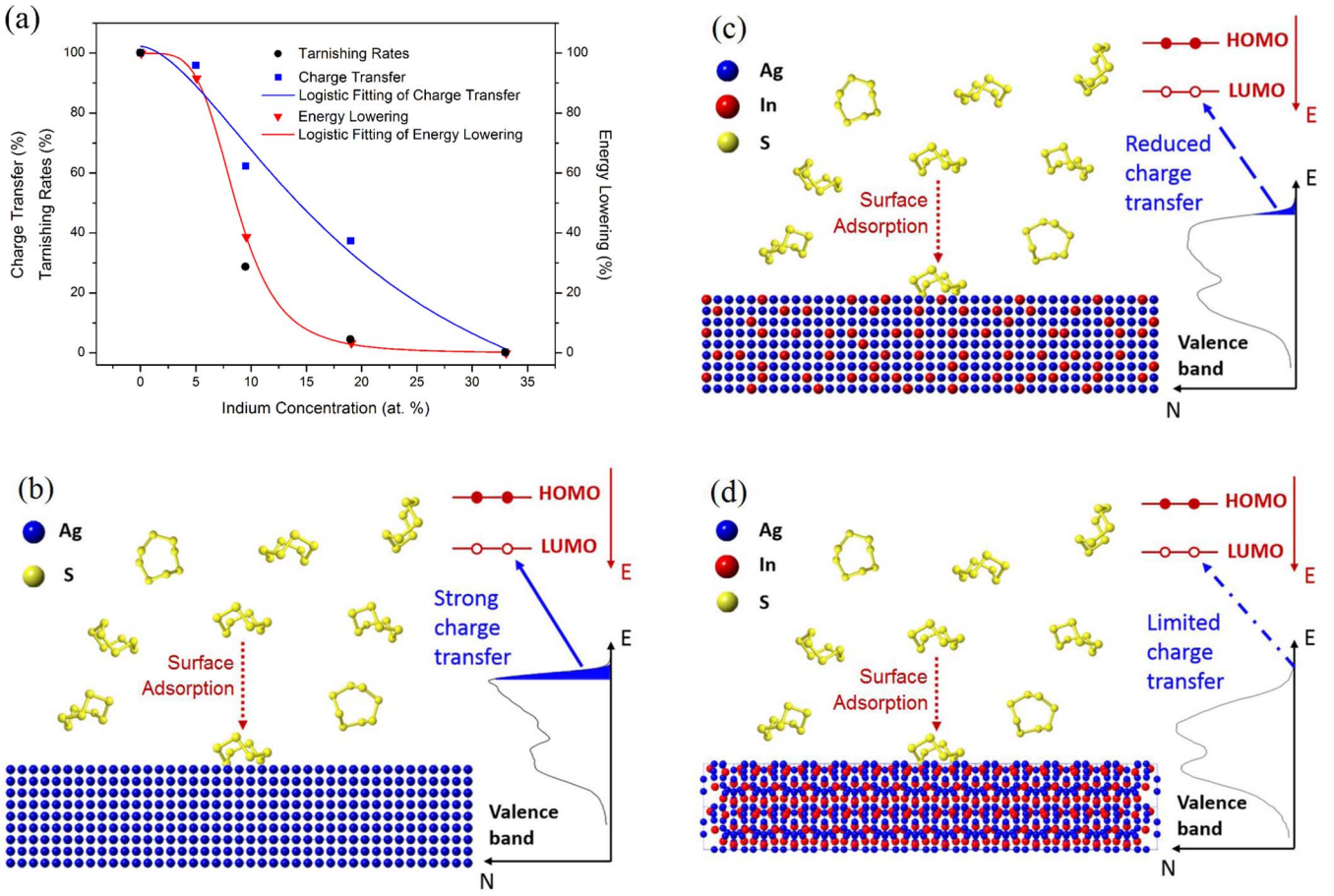

Figure 7. (a) The plot of logistic fitting curves for calculated total charge transfer and energy lowering of reactions with S_2 molecule and experimental reactions rates with S_8 molecule, (b) schematic diagram of Ag tarnishing mechanism, (c) Ag-In solid solution anti-tarnishing mechanism and (d) Ag_9In_4 IMC anti-tarnishing mechanism.

with anti-tarnishing mechanism at this point, or at least, it is not the determining factor for the anti-tarnishing mechanism in the Ag-In binary system.

Concluding Remarks

Anti-tarnishing mechanism in silver-indium has been investigated, and the nature of tarnishing and anti-tarnishing phenomena has been advanced. It could be one step further toward the development of ultimate remedy for silver tarnishing issues and meaningful for corrosion inhibitor design. With the scientific knowledge of anti-tarnishing mechanism, it could serve as a design guidance in principle for the practical applications of Ag-In alloy bulk or thin film materials into various fields, such as electrical and mechanical interconnections of SiC/GaN-based power electronics, GaN-based LED reflector, giant astronomical telescope array of mirrors construction etc.

In summary, the anti-tarnishing mechanism in the silver-indium binary system has been explored by fabricating and experimental characterization of thin film samples using GIXRD, XPS and UPS techniques. An alternative method was used to calculate the absolute electronegativity and chemical hardness for bulk metals within the framework of the HSAB principle and its conceptual DFT formalization, using measured UPS spectra data of valence band structures. The absolute electronegativity and chemical hardness both increase in the Ag-In binary system as the indium concentration increases, which explains the underlying anti-tarnishing mechanism in terms of the soft acid–soft base electron charge transfer and energy lowering process. The calculation results are in accordance with the theoretical predictions of reactivity of metal surface given by the Hammer-Nørskov d-band model. Essentially, this methodology is a semi-quantum-mechanical approach applying theoretical thermodynamic calculations while using experimental data obtained from metallic valence bands measurement. Therefore, it is an experimentally driven quantum-mechanical investigation, rather than computationally model driven. However, this HSAB calculation recipe can be readily used for the DFT computational software calculated DOS. It could be further developed and generalized to apply to other metallic systems for noble and transition metals, since it largely correlated with the Hammer-Nørskov d-band model. It would also have potential applications in the field of valence-band engineering[67–70] for corrosion resistant alloys design. In other words, this semi-quantum-mechanical methodology is an alternative application to the HSAB principle chemical analysis in calculating, explaining, and predicting thermodynamic and reactivity behaviors for metallic materials.

Acknowledgment

The authors would like to express our gratitude for the film deposition work performed at the UC Irvine Materials Research Institute (IMRI) using instrumentation funded by DURIP award FA2386-14-1-3026, GIXRD works preformed in IMRI using Rigaku SmartLab X-ray diffractometer, and the XPS/UPS work done in IMRI using instrumentation funded in part by the National Science Foundation Major Research Instrumentation Program under grant no. CHE-1338173. The authors declare no competing financial interest.

References

1. D. Kagan, *American Journal of Archaeology*, **86** (3), 343 (1982).
2. L. Ke, S. C. Lai, H. Liu, C. K. N. Peh, B. Wang, and J. H. Teng, *Acs. Appl. Mater. Inter.*, **4** (3), 1247 (2012).
3. Y. L. Wu, Y. N. Li, and B. S. Ong, *J. Am. Chem. Soc.*, **129** (7), 1862 (2007).
4. C. C. Yu, J. D. Baek, C. H. Su, L. D. Fan, J. Wei, Y. C. Liao, and P. C. Su, *Acs. Appl. Mater. Inter.*, **8** (16), 10343 (2016).
5. K. Awazu, M. Fujimaki, C. Rockstuhl, J. Tominaga, H. Murakami, Y. Ohki, N. Yoshida, and T. Watanabe, *J. Am. Chem. Soc.*, **130** (5), 1676 (2008).
6. S. Dunn, P. M. Jones, and D. E. Gallardo, *J. Am. Chem. Soc.*, **129** (28), 8724 (2007).
7. G. V. Ramesh and T. P. Radhakrishnan, *Acs. Appl. Mater. Inter.*, **3** (4), 988 (2011).
8. A. Dabirian and N. Taghavinia, *Acs. Appl. Mater. Inter.*, **7** (27), 14926 (2015).
9. Y. T. Chen, T. Q. Yang, H. F. Pan, Y. F. Yuan, L. Chen, M. W. Liu, K. Zhang, S. J. Zhang, P. Wu, and J. H. Xu, *J. Am. Chem. Soc.*, **136** (5), 1686 (2014).
10. P. Peng, A. M. Hu, A. P. Gerlich, G. S. Zou, L. Liu, and Y. N. Zhou, *Acs. Appl. Mater. Inter.*, **7** (23), 12597 (2015).
11. M. Maruyama, R. Matsubayashi, H. Iwakuro, S. Isoda, and T. Komatsu, *Appl. Phys. a-Mater.*, **93** (2), 467 (2008).
12. B. T. Reagor and J. D. Sinclair, *J. Electrochem. Soc.*, **128** (3), 701 (1981).
13. H. Kim, *Mater. Corros.*, **54** (4), 243 (2003).
14. M. Xiuying and T. Kaishang, *Electroplating & Pollution Control*, **15**(1), 8 (1995).
15. J. D. Sinclair, *J. Electrochem. Soc.*, **129**(1), 33 (1982).
16. M. H. Hebb, *J. Chem. Phys.*, **20**(1), 185 (1952).
17. G. Mura, G. Cassanelli, F. Fantini, and M. Vanzi, *Microelectron. Reliab.*, **48** (8), 1208 (2008).
18. D. Minzari, M. S. Jellesen, P. Moller, and R. Ambat, *Eng. Fail. Anal.*, **18**(8), 2126 (2011).
19. T. E. Graedel, *J. Electrochem. Soc.*, **139**(7), 1963 (1992).
20. C. J. Yang, C. H. Liang, and X. Liu, *Anti-Corros. Method. M*, **54**(1), 21 (2007).
21. R. R. Benham, *Anti-Corros. Method.M*, **10**(2), 31 (1963).
22. R. Bond, R. P. Stanek, and W. Hoffman, *US 5834103*, November 10, 1998.
23. L. Paussa, L. Guzman, E. Marin, N. Isomaki, and L. Fedrizzi, *Surf. Coat. Tech.*, **206**(5), 976 (2011).
24. C. H. Liang, C. J. Yang, and N. B. Huang, *Surf. Coat. Tech.*, **203**(8), 1034 (2009).
25. J. P. Randin, *Werkst. Korros.*, **43**(4), 172 (1992).
26. J. Nielsen and J. Tuccillo, *US 3767391*, October 23, 1973.
27. S. Nisaratanaporn and E. Nisaratanaporn, *Journal of Metals, Materials and Minerals*, **12**(2), 13 (2003).
28. K. F. Edward, *US 1970319*, August 14, 1934.
29. P. Johns, *US 20070009375*, January 11, 2007.
30. D. Davitz, *US 5882441*, March 16, 1999.
31. Y. J. Huo, S. W. Fu, Y. L. Chen, and C. C. Lee, *J. Mater. Sci.-Mater. El.*, **27**(10), 10382 (2016).
32. Y. J. Huo and C. C. Lee, *J. Alloy. Compd.*, **661** 372 (2016).
33. C. S. Fadley and D. A. Shirley, *J. Res. Nbs. a Phys. Ch., A*, **74**(4), 543 (1970).
34. W. Hume-Rothery, G. F. Lewin, and P. W. Reynolds, *Proc. R Soc. Lon. Ser.-A*, **157**(A890), 0167 (1936).
35. S. Doniach and M. Sunjic, *J. Phys. Part C Solid*, **3**(2), 285 (1970).
36. A. Barrie and N. E. Christensen, *Phys. Rev. B*, **14**(6), 2442 (1976).
37. I. A. Abrikosov, W. Olovsson, and B. Johansson, *Phys Rev Lett*, **87**(17), 176403-4 (2001).
38. B. Johansson and N. Martensson, *Phys. Rev. B*, **21**(10), 4427 (1980).
39. P. Steiner and S. Hüfner, *Acta Metallurgica*, **29**(11), 1885 (1981).
40. A. Rosengren and B. Johansson, *Phys. Rev. B*, **23**(8), 3852 (1981).
41. U. Gelius, *Phys. Scripta*, **9**(3), 133 (1974).
42. A. I. Boronin, S. V. Koscheev, and G. M. Zhidomirov, *J. Electron. Spectrosc.*, **96** (1), 43 (1998).
43. C. Donley, D. Dunphy, D. Paine, C. Carter, K. Nebesny, P. Lee, D. Alloway, and N. R. Armstrong, *Langmuir*, **18**(2), 450 (2002).
44. M. Trzcinski, A. Bukaluk, M. Burgener, and A. Goldmann, *Surf. Sci.*, **589** (1), 192 (2005).
45. J. Riley, R. Leckey, J. Jenkin, J. Liesegang, and R. Poole, *Journal of Physics F: Metal Physics*, **6**(2), 293 (1976).
46. G. Panaccione, G. Cautero, M. Cautero, A. Fondacaro, M. Grioni, P. Lacovig, G. Monaco, F. Offi, G. Paolicelli, M. Sacchi, N. Stojic, G. Stefani, R. Tommasini, and P. Torelli, *J Phys-Condens Mat*, **17**(17), 2671 (2005).
47. B. Hammer and J. K. Nørskov, *Adv. Catal.*, **45**, 71 (2000).
48. B. Hammer, *Topics Catal*, **37**(1), 3 (2006).
49. R. G. Pearson, *J. Am. Chem. Soc.*, **85**(22), 3533 (1963).
50. R. G. Pearson, *Inorg. Chem.*, **27**(4), 734 (1988).
51. T. -L. Ho, *Chemical Reviews*, **75**(1), 1 (1975).
52. R. G. Pearson, *J. Chem. Educ.*, **45**(10), 643 (1968).
53. J. Chatt and L. M. Venanzi, *Nature*, **177**(4514), 852 (1956).
54. R. S. Mulliken, *J. Am. Chem. So*,c., **77**(4), 884 (1955).
55. R. G. Pearson, *J. Chem. Educ.*, **64**(7), 561 (1987).
56. R. G. Parr and R. G. Pearson, *J. Am. Chem. Soc.*, **105**(26), 7512 (1983).
57. W. Kohn, A. D. Becke, and R. G. Parr, *J. Phys. Chem.-Us*, **100**(31), 12974 (1996).
58. R. G. Parr, R. A. Donnelly, M. Levy, and W. E. Palke, *The Journal of Chemical Physics*, **68**(8), 3801 (1978).
59. M. H. Cohen and A. Wasserman, *J. Phys. Chem. A*, **111**(11), 2229 (2007).
60. J. P. Perdew, R. G. Parr, M. Levy, and J. L. Balduz, *Phys. Rev. Lett.*, **49**(23), 1691 (1982).
61. U. Salzner and R. Baer, *The Journal of Chemical Physics*, **131**(23), 23110-1-4 (2009).
62. A. L. Allred, *J. Inorg. Nucl. Chem.*, **17**(3–4), 215 (1961).
63. W. Yang and R. G. Parr, *Proc. Natl. Acad. Sci. USA*, **82**(20), 6723 (1985).
64. L. Lee, *J. Adhesion. Sci. Technol.*, **5**(1), 71 (1991).
65. A. Kokalj, *Chem. Phys.*, **393**(1), 1 (2012).
66. S. Lilienfeld and C. E. White, *J. Am. Chem. Soc.*, **52**, 885 (1930).
67. L. D. Zhao, J. Q. He, S. Q. Hao, C. I. Wu, T. P. Hogan, C. Wolverton, V. P. Dravid, and M. G. Kanatzidis, *J. Am. Chem. Soc.*, **134**(39), 16327 (2012).
68. G. J. Tan, L. D. Zhao, F. Y. Shi, J. W. Doak, S. H. Lo, H. Sun, C. Wolverton, V. P. Dravid, C. Uher, and M. G. Kanatzidis, *J. Am. Chem. Soc.*, **136**(19), 7006 (2014).
69. G. J. Tan, F. Y. Shi, S. Q. Hao, H. Chi, T. P. Bailey, L. D. Zhao, C. Uher, C. Wolverton, V. P. Dravid, and M. G. Kanatzidis, *J.Am. Chem. Soc.*, **137**(35), 11507 (2015).
70. A. Banik, U. S. Shenoy, S. Saha, U. V. Waghmare, and K. Biswas, *J. Am. Chem. Soc.*, **138**(39), 13068 (2016).